



OPEN ACCESS

EDITED BY

Yingwei Wang,
Huashan Hospital of Fudan University,
China

REVIEWED BY

Xiao-Qing Tang,
University of South China, China
Changjun Gao,
Fourth Military Medical University, China

*CORRESPONDENCE

Tianlong Wang
w_tl5595@hotmail.com

[†]These authors have contributed equally to this work and share first authorship

SPECIALTY SECTION

This article was submitted to Neurocognitive Aging and Behavior, a section of the journal Frontiers in Aging Neuroscience

RECEIVED 07 August 2022

ACCEPTED 10 October 2022

PUBLISHED 17 November 2022

CITATION

Liu Y, Feng H, Fu H, Wu Y, Nie B and Wang T (2022) Altered functional connectivity and topology structures in default mode network induced by inflammatory exposure in aged rat: A resting-state functional magnetic resonance imaging study.
Front. Aging Neurosci. 14:1013478.
doi: 10.3389/fnagi.2022.1013478

COPYRIGHT

© 2022 Liu, Feng, Fu, Wu, Nie and Wang. This is an open-access article distributed under the terms of the [Creative Commons Attribution License \(CC BY\)](https://creativecommons.org/licenses/by/4.0/). The use, distribution or reproduction in other forums is permitted, provided the original author(s) and the copyright owner(s) are credited and that the original publication in this journal is cited, in accordance with accepted academic practice. No use, distribution or reproduction is permitted which does not comply with these terms.

Altered functional connectivity and topology structures in default mode network induced by inflammatory exposure in aged rat: A resting-state functional magnetic resonance imaging study

Yang Liu^{1,2†}, Huiru Feng^{1†}, Huiqun Fu¹, Yan Wu³, Binbin Nie⁴ and Tianlong Wang^{1,2*}

¹Department of Anesthesiology, Xuanwu Hospital, Capital Medical University, Beijing, China, ²National Clinical Research Center for Geriatric Diseases, Beijing, China, ³Department of Anatomy, Capital Medical University, Beijing, China, ⁴Institute of High Energy Physics, Chinese Academy of Sciences, Beijing, China

Inflammatory stress in anesthesia management and surgical process has been reported to induce long-term cognitive dysfunction in vulnerable aged brain, while few studies focused on the network mechanism. The default mode network (DMN) plays a significant role in spontaneous cognitive function. Changes in topology structure and functional connectivity (FC) of DMN in vulnerable aged brain following inflammatory stress-induced long-term cognitive dysfunction are rarely studied. Eighty-eight aged male rats received intraperitoneal injection of lipopolysaccharide (LPS) as treatment or equal amount of normal saline (NS) as control. Morris Water Maze (MWM) was performed to assess short- (<7 days) and long-term (>30 days) learning and spatial working memory. Enzyme-linked immunosorbent assay (ELISA) was used to measure systemic and hippocampus inflammatory cytokines. Real-time polymerase chain reaction (RT-PCR) was used to measure the changes in gene level. Resting-state functional magnetic resonance imaging (rs-fMRI) was used to exam brain function *prior* to MWM on days 3, 7, and 31 after LPS exposure. Graph theory analysis was used to analyze FC and topology structures in aged rat DMN. Aged rats treated with LPS showed short- and long-term impairment in learning and spatial working memory in MWM test. Graph theory analysis showed temporary DMN intrinsic connectivity increased on day 3 followed with subsequent DMN intrinsic connectivity significantly altered on day 7 and day 31 in LPS-exposed rats as compared with controls. Short- and long-term alterations were observed in FC, while alterations in topology structures were only observed on day 3. Rats with inflammatory stress exposure may cause short- and long-term alterations in intrinsic connectivity in aged rat's DMN while the changes in topology structures only lasted for 3 days. Inflammatory stress has prolonged effects on FC, but not topology structures in venerable aged brain.

KEYWORDS

anesthesia, inflammation, cognitive dysfunction, default mode network, small worldness

Introduction

Cognitive dysfunction following anesthesia and surgery is widely reported in clinical practice (Belrose and Noppens, 2019; Liu et al., 2022). Among the population, elderly patients were shown to be more vulnerable to neuroinflammation induced by anesthesia neurotoxicity and surgical trauma, which may further develop into long-term cognitive dysfunction (Daiello et al., 2019). Surgical trauma is recently believed to be a major source for inflammatory cytokines in clinical practice (Yang T. et al., 2020; Liu et al., 2022). Clinical study has shown that the postoperative cognitive decline is associated with increased mortality (Yang T. et al., 2020; Duprey et al., 2021; Liu et al., 2022). In this case, understanding how the cognitive impaired aged brain functions in such conditions is of great significance for disease prevention and drug target design, as well as a better perioperative outcome for elderly patients.

Traditional neuroscience approaches mainly focused on several localized regions (e.g., hippocampus and prefrontal cortex; Lisman et al., 2017; Le Merre et al., 2021) to make a detailed experiment in particular animal models. However, as none of the cognitive function can be fully understood if taken out of a broad connectionist context (Fuster, 2001) and the brain functions as networks instead of separate regions in living subjects (Avena-Koenigsberger et al., 2017), results from traditional approaches may only provide limited evidence in disease mechanism and development. Recent studies reported the significance of “neural network disease,” as the functions of neural network and topology changes contributed largely to disease development and revealed medical treatment outcomes (Zhang et al., 2021; Kukla et al., 2022). These results highly emphasized the importance of understanding how the neural network changes during inflammatory exposure induced cognitive decline in a broad scale in living brain.

Resting-state functional magnetic resonance imaging (rs-fMRI), which measures spontaneous brain activity *via* low frequency fluctuations in blood-oxygen-level-dependent (BOLD) signal, provides a non-invasive method to study brain function in living subjects (Biswal et al., 1995). By abstracting brain networks as graphs, the graph theory method analyzed BOLD signal by dividing the brain networks into different elements (nodes) and their pairwise links (edges). Brain nodes are neurons/entire brain regions and edges are binary/weighted values (Sporns, 2018). Functional connectivity (FC), defined as correlations (edges in the graph) of neuronal activation between different brain regions (nodes in the graph), has been shown to be modulated in various diseases conditions (Ji et al., 2018; Liu et al., 2018; Schumacher et al., 2021). Meanwhile,

topology properties and intrinsic connectivity of brain networks may also be altered in disease situations (Lopes et al., 2017; Lee et al., 2019). In this way, by considering topology properties and FC in a whole scale, rs-fMRI and graph theory method provide a detailed understanding of changes in brain networks, indicating an optional choice for studying disease mechanisms.

The default mode network (DMN) is a set of widely distributed brain regions, which often show reductions in activity during attention-demanding tasks but increase their activity across multiple forms of complex cognition. Many of which are linked to memory or abstract thought (Smallwood et al., 2021). Impaired FC in DMN has been characterized as one of the major changes in patients with Alzheimer’s disease (AD) and mild cognitive impairment (MCI; Chand et al., 2017; Hohenfeld et al., 2018; Cao et al., 2020), demonstrating a potential use for FC in DMN in cognitive function. Recent data from preclinical experiments have shown that the DMN not only exists across species but also similar in components (Li and Zhang, 2018; Jing et al., 2021; Yeshurun et al., 2021), suggesting that study of DMN in rodent models would be applicable in investigating mechanisms of human diseases. Although there are studies demonstrating changes in DMN in A β -induced cognitive decline (Pascoal et al., 2019), few studies focused on the DMN alteration in acute- and long-term after inflammatory stress exposure.

This study is designed to investigate acute and long-term changes in DMN after inflammatory stress exposure in anesthesia process. Inflammatory stress was induced by lipopolysaccharide (LPS) injection, as it is one of the most widely used initiators for inducing systemic inflammatory responses and cognitive decline (Kan et al., 2016; Lakshmikanth et al., 2016; Yang L. et al., 2020) in preclinical experiments. Aged rats were used in this experiment because elderly patients are at highly risk for cognitive dysfunction after anesthesia and surgery (Belrose and Noppens, 2019). The model was adapted from our previous work, which demonstrated that a single intraperitoneal injection of LPS (2 mg/kg) induces a long-term inflammatory response in aged rat hippocampus and impaired behavior performances (Fu et al., 2014; Kan et al., 2016). Systemic levels of inflammatory cytokines, including interleukin-1 β (IL-1 β) and tumor necrosis factor-alpha (TNF α), were measured by enzyme-linked immunosorbent assay (ELISA) as their levels are highly correlated with sickness behavior after LPS exposure (Oliveira et al., 2020). We hypothesized that the topology structure and FC in the aged rat DMN will both change after inflammatory exposure, which may provide new insights into drug target design and new diagnostic biomarkers.

Materials and methods

Ethics approval

All animal procedures were approved by the Ethical Committee of Capital Medical University as complied with the guide for Care and Use of Laboratory Animals prepared by the Institute of Laboratory Animal Resources and published by the National Institute of Health. All efforts were made to minimize the pain and suffering of the animals.

Animal preparations

A total of 88 adult male Wistar rats (19 months, 650–800 g, Charles-River Animal Technology, Beijing, China) were housed in an animal facility under a 12/12 light–dark cycle at $22 \pm 2^\circ\text{C}$ with 50%–60% humidity. Food and water were available *ad libitum*.

Rats were intraperitoneally injected (i.p.) with either lipopolysaccharide (LPS, 055: B5, Sigma-Aldrich, St Louis, MO, United States) or sterilized normal saline (NS, OC90F1, Otsuka Pharmaceutical, Co, Ltd., Beijing, China) and were allocated to either LPS group ($n = 60$, 2 mg/kg, i.p.) or NS group ($n = 28$, same volume with LPS solution injection). The dose for LPS was adapted from our previous work which showed that low-dose LPS injection caused prolonged cognitive dysfunction in aged rat (Figure 1A; Fu et al., 2014; Kan et al., 2016).

Morris water maze

All rats ($n = 12$ in each group) performed MWM test with the protocols adopted from our previous work (Kan et al., 2016). The MWM is a circular tank placed in a quiet and dimly lit room with visual clues around. The inner surface of the tank was painted in black and filled with water ($24 \pm 1^\circ\text{C}$) in about 20 cm in depth. A hidden platform was placed in one fixed quadrant hidden in about 1.5 cm below the water surface. On top of the circular tank is a video camera tracking the behavior performance of the rats. Around the circular tank is a series of large support holders with thick curtains to avoid sharp lights if necessary. Briefly, the MWM test contains two sections of spatial acquisition trials (day 1–5 and day 31–35) and probe trials (day 7 and day 37) to assess learning and spatial working memory in both short term (<7 days) and long term (>30 days). For the spatial acquisition trial, the rat was gently placed in one of the quadrants facing the wall of MWM circular pool and then was allowed to swim freely for 60 s to find the hidden platform. If the rat succeeds, it was allowed to stay on the platform for 5 s. Otherwise, it would be manually placed on the platform and allowed to stay for 20 s. Four spatial acquisition trials were performed in each day to let the rat entering the MWM from four different quadrants and the training session lasted for 5 consecutive days. On day 7, a probe trial was performed with the

hidden platform removed. Rats were gently placed in the opposite quadrant to the original location of the platform and allowed to swim freely for 30 s. On day 6, the rats were allowed to have a rest. The latency to find the platform in spatial acquisition trials and the time spent and crossovers in platform quadrant in probe trials were recorded and analyzed using an animal behavior tracking system (EthoVision, Noldus Information Technologies, Netherlands). From days 31 to 35, another section of spatial acquisition trials was repeated followed with another probe trial on day 37. After finishing the behavior examination, the rats were sacrificed by over inhalation of isoflurane (ISO) with injection of potassium *via* the femoral vein. The timeline for MWM protocol is summarized in Figures 1B, 2A.

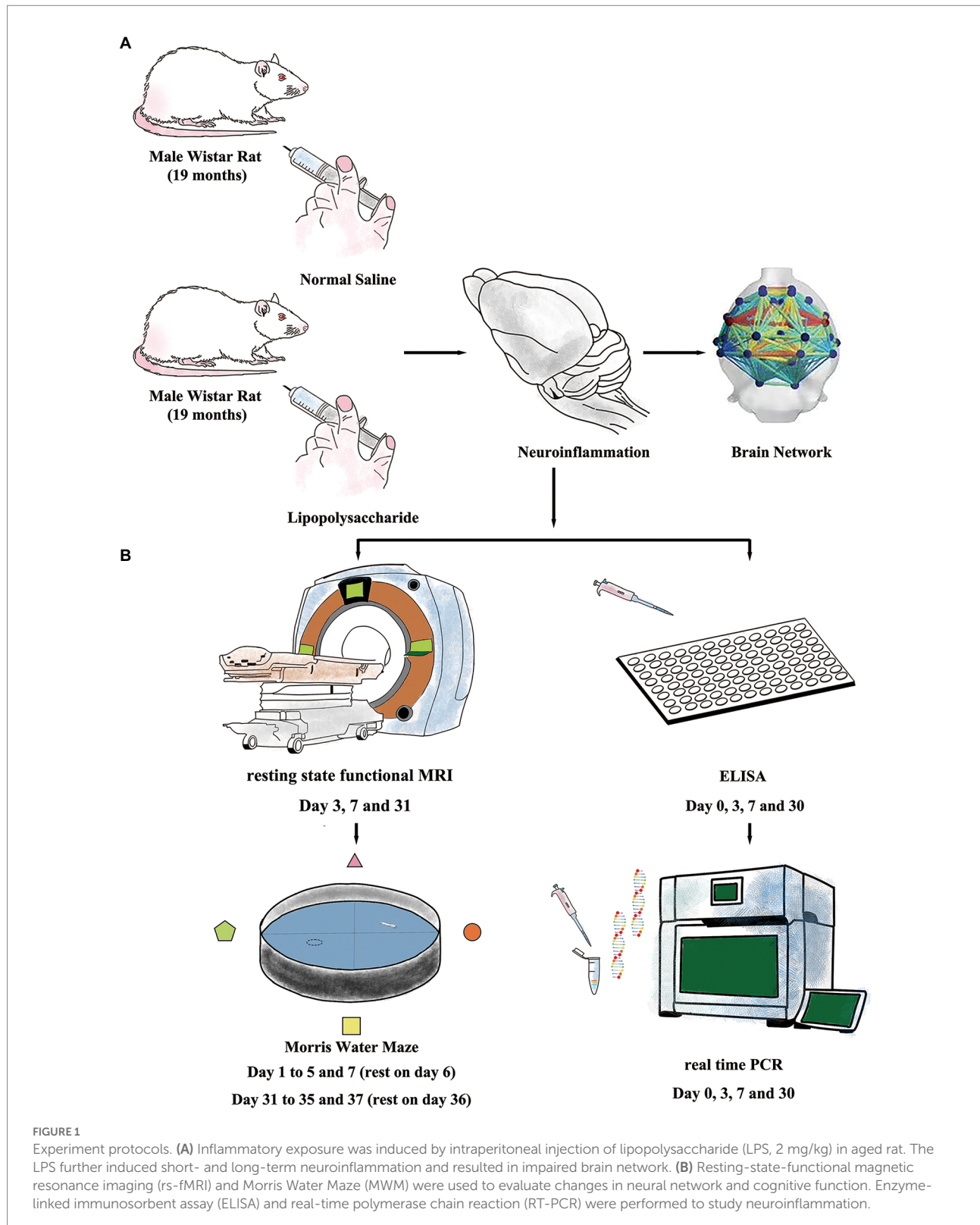
Tissue preparation

On day 0 (before LPS or NS treatment, baseline), and days 3, 7, and 30 after LPS exposure, a cohort of animals ($n = 8$ for each time point each group) was selected for inflammatory cytokine examination. On the day of termination, rats were anesthetized by isoflurane (ISO, Baxter, Lessines, Belgium) prior to *vena cava* blood sampling (5 ml for each time). After 2 h of clotting at 4°C , blood samples were subjected to centrifugation at 1,000g for 20 min and the serum was later collected and stored at -80°C .

After decapitation, rat brain was quickly dissected and dividing by half using a chilled cold blade. The left part of the brain was rapidly grinded into small pieces and then homogenized by the RIPA Lysis Buffer (P0013C, Beyotime, Beijing, China) at the concentration of 20 mg tissue/200 μg buffer. Prior to homogenization, PMSF (100 mM, P0100-1, Solarbio, Beijing, China) was added to the RIPA lysis buffer to reach the concentration of 1 mM/ml. After centrifugation (Eppendorf, Centrifuge 5810R, China) at 1,000g, 4°C for 20 min, the supernatant was collected and stored at -80°C for further use.

mRNA and RT-PCR

For the same rat, the right part of the brain was used for operating this procedure. Total RNA was extracted from hippocampus by Trizol reagent (Invitrogen, Paisley, United Kingdom) and was purified by the RNase Away Reagent (catalog number 18270466, Invitrogen, Paisley, United Kingdom). Prior the RT-PCR process, the integrity of mRNA was measured by NanoDrop 2000 (Thermo Scientific, Waltham, MA, United States) and the cDNA was synthesized by the M-MLV Reverse Transcriptase Kit according to the manufacturer's instructions. The cDNA amplification was operated by the ABI 7500 Fast Real-Time PCR System (Applied Biosystems, Waltham, MA, United States) for 45 cycles (each for a duration of 2 min at 94°C , annealing for 5 s at 94°C and then for 30 s at 60°C and finally extension for 10 min at 72°C). The primer and amplification



sequences for IL-1 β , TNF α , and NF- κ B were shown in Table 1. The level of mRNA expression was calculated by the SYBR Green direction method, and all the data were analyzed by the $2^{-\Delta\Delta Ct}$ method by the target gene expression in rat cortex corrected by β -actin expression.

Enzyme-linked immunosorbent assay measurements

On day 0 (before LPS or NS treatment), and days 3, 7, and 30 after LPS exposure, a cohort of animals ($n=8$ for each time point

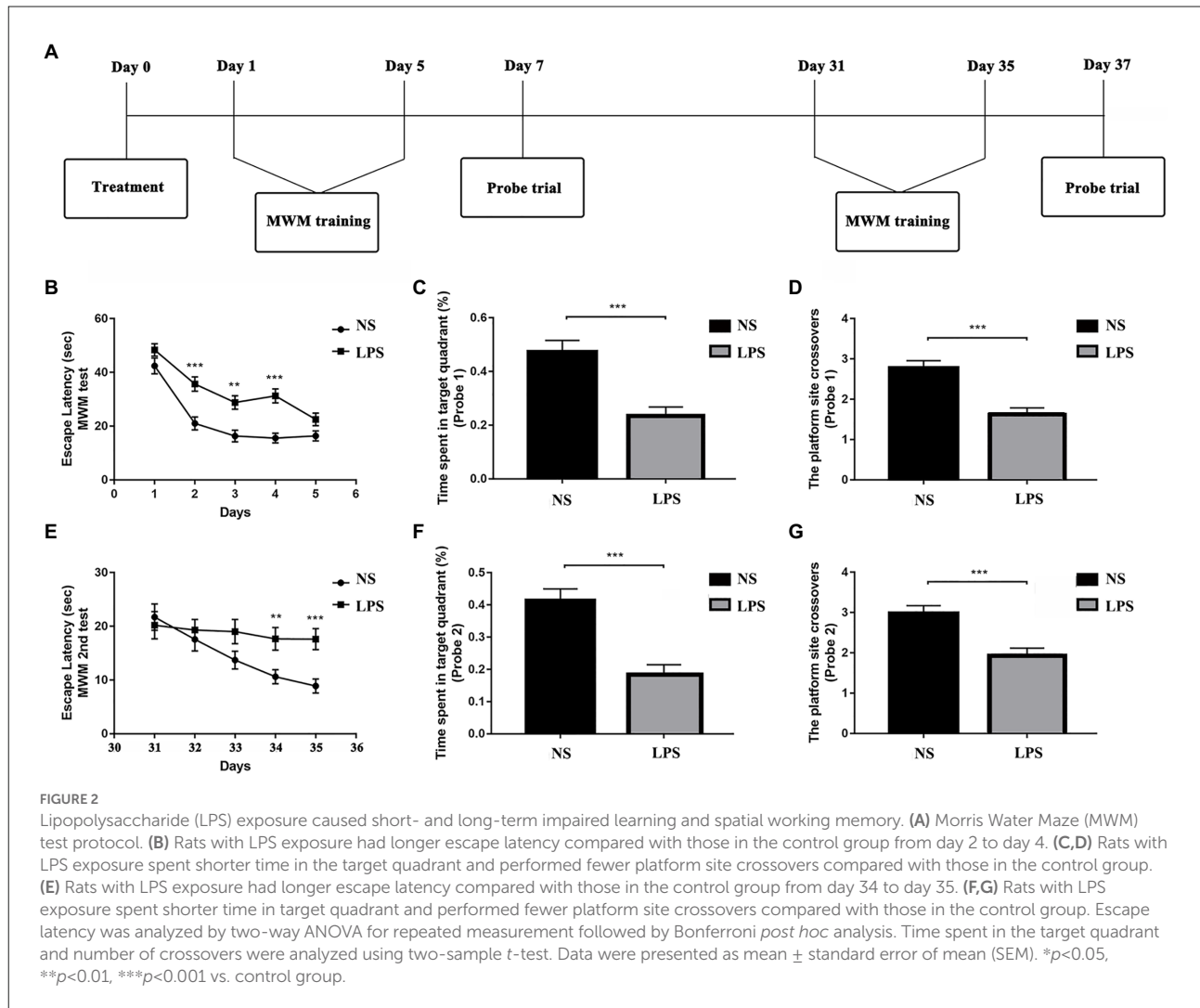


TABLE 1 Primer sequences in RT-PCR.

mRNA	Forward primer (5' → 3')	Reverse primer (5' → 3')
IL-1 β	5'-ATGAGAGCATCCAGCTTCAAATC-3'	5'-CACACTAGCAGGTGTCATCATC-3'
TNF α	5'-CAAGAGCCCTTGCCCTAA-3'	5'-CAGAGCAATGACTCCAAAGTA-3'
NF- κ B	5'-AATTTGGCTTCCTTCTTGGCT-3'	5'-CTGCATACCTTAATGACACG-3'
β -actin	5'-CCCATCTATGAGGGTTACGC-3'	5'-TTAATGTCACGCACGATTTC-3'

each group) was selected for inflammatory cytokine examination (Figure 1). On the day of termination, rats were anesthetized by isoflurane (ISO, Baxter, Lessines, Belgium) prior to *vena cava* blood sampling. After 2h of clotting at 4°C, the blood was centrifuged at 1,000g for 20 min and the serum was later collected and stored at -80°C. IL-1 β and TNF α levels were measured using ELISA assay kits (RLB00 and RTA00, R&D Systems, Inc., Minneapolis, MN, United States) according to manufacturer instructions.

Anesthesia on rats

The protocols for anesthesia have been published by Liu et al. elsewhere (Lu et al., 2012). Briefly, all rats were first induced by ISO at the concentration of 3% followed by intramuscular injection of dexmedetomidine (DEX, Hengrui Medicine Co., Ltd., Jiangsu Province, China, 0.015 mg/kg). During the initial scanning, ISO (1%) in oxygen-enriched air was delivered *via* a customized nose cone with continuous intramuscular infusion of

DEX (0.03 mg/kg/h). After the anatomical localization scans were acquired, the ISO concentration was decreased to 0.20%–0.25% with the respiration rate maintained at 60–85/min. When the respiration rate increased to 90/min, ISO concentration was adjusted to 0.5%. A small animal monitoring system (Model 1025, Small Animal Instruments Inc., New York, NY, United States), including a rectal temperature probe, respiration pneumatic sensor, and fiber optic oximetry sensor or cardiogram electrodes, was adopted for real-time monitoring. The core body temperature was maintained at 37°C *via* a warm water circulation system on the scanning bed.

Magnetic resonance imaging

Animals to perform rs-fMRI ($n=10-12$ for each group) scanning also performed MWM examination in order to minimize individual variations between rs-fMRI data and behavior performance. The rs-fMRI scanning was performed on days 3, 7, and 31 post-treatment and *prior to* the MWM test. (Figure 1B).

The animal MRI measurements were performed using the 7.0T Bruker PharmaScan System (70/16 PharmaScan, Bruker Biospin GmbH, Germany), operated *via* the ParaVision 5.1 software. The same coils, including a rat brain surface coil and a quadrature resonator volume coil, were adopted in all rats.

Anatomical images (T2WI) were acquired with fast-spin-echo sequence using TurboRARE with the following parameters: repetition time (TR) 5000.0 ms, echo time (TE) 36.0 ms, echo spacing 12 ms, echo-train length 8, field of view 3.50×3.50 cm, matrix size 256×256 , and 28 slices with a thickness of 1.0 mm. For blood-oxygen-level-dependent (BOLD) images, EPI-SE-FOVsat sequence was used with the following parameters: matrix size 64×64 , flip angle = 90° , resolution = $0.55 \text{ mm} \times 0.55 \text{ mm}$, 28 slices with a thickness of 1.0 mm, slice gap = 0, repetition time (TR) = 2000.0 ms, echo time (TE) = 18.0 ms, and volume = 180.

Data processing and analysis

The data were pre-processed using spmratIHEP software (Nie et al., 2013; Liang et al., 2017) based on the statistical parametric mapping (SPM12; Wellcome Department of Imaging Science)¹ and GRETNA software² based on the Matlab (version 2014a, The MathWorks Inc., Natick, MA, United States). The data were carefully examined for completeness and truncation artifacts. All the functional images post-processing was performed by a single experienced observer, unaware to whom the scans belonged.

The voxel size of the functional datasets of all individuals was first multiplied by a factor of 5 to better approximate human dimensions, and then slice timing and realigning were performed.

In the slice-timing section, the difference of slice acquisition times of each subject was corrected. Then, the realignment was done by adjusting the temporal-processed volume of each subject to the first volume in order to remove the head motion. After this, a mean image over the 180 volumes was recreated. In this section, data from subjects were filtered and preserved by which a 1 mm of translation in the x , y , or z axis and a 1° of rotation in each axis were set as criteria. Otherwise, it was eliminated. After spatial normalization into the Paxinos and Watson space, all the normalized images were re-sliced by $1.0 \times 1.5 \times 1.0 \text{ mm}^3$ voxels (after zooming). Then the normalized functional series were smoothed with a Gaussian kernel of 2 mm^3 Full Width at Half-maximum (FWHM) and the systematic drift or trend was removed using a linear model. Finally, the linear trended images were 0.01–0.08 Hz band-pass filtered and further corrected for the effect of head movement by regressing the translations and rotations of the head estimated during image realignment.

For default mode network (DMN) analysis, 12 regions of interest (ROIs; comprising left/right segmentation) were selected from the rat brain atlas image in Paxinos and Watson space (Nie et al., 2013; Liang et al., 2017). All these ROIs were summarized in Table 2.

These ROIs were defined as nodes and functional connectivity (FC) was defined as the Pearson's correlation coefficients (CCs) between each pair of nodes and calculated in GRETNA. Weighted undirected 12×12 matrices were constructed for LPS and NS groups for each time point mentioned above, in which the strength of each connection was presented as FC.

Graph theory analysis

Based on the weighted matrix, distance matrices of the above two groups were generated, where the distance between each node was defined as $L_{ij} = 1 - w_{ij}$. The L_{ij} was identified as connection weight in nodes i and j .

TABLE 2 Region of interest in aged rat brain.

Region of interest (ROI)	ROI index	Short-form
01_Auditory cortex_Left	1	L_AC
02_Auditory cortex_Right	2	R_AC
03_Hippocampus_Left	3	L_Hip
04_Hippocampus_Right	4	R_Hip
05_Orbital cortex_Left	5	L_OC
06_Orbital cortex_Right	6	R_OC
07_Parietal association cortex_Left	7	L_PAC
08_Parietal association cortex_Right	8	R_PAC
15_Prelimbic cortex_Left	9	L_PrC
16_Prelimbic cortex_Right	10	R_PrC
17_Retrosplenial cortex_Left	11	L_RSC
18_Retrosplenial cortex_Right	12	R_RSC

All the ROIs were drawn according to the Paxinos and Watsons space, with 12 ROIs (comprising left/right segmentation) were selected.

¹ <http://www.fil.ion.ucl.ac.uk/spm>

² <https://www.nitrc.org/projects/gretna/>

Graph theoretical analysis using Gretna Toolbox³ was adopted to characterize FC patterns in group LPS and NS. For further analysis, global efficiency (E_{glob}) and local efficiency (E_{loc}) were used to assess network efficiency while nodal efficiency (E_i) and nodal local efficiency (E_{i_local}) were used to assess nodal centralities of the neural network. Based on graph theory, E_{global} is defined as the harmonic mean of the minimum path length between all possible pairs of nodes in neural network. E_{loc} is defined as the local efficiency of sub-graph composed of the neighbors of node i . E_i is defined as the ability of a node to propagate information with the other nodes in a network. E_{i_local} is defined as the efficiency of information propagation over a node's direct neighbors (Wang et al., 2010). The mathematical definitions are characterized as the following:

$$E_{glob}(G) = \frac{1}{N(N-1)} \sum_{i \neq j \in G} \frac{1}{L_{i,j}}, E_{loc} = \frac{1}{N} \sum_{i \in G} E_{glob}(G_i), E_i = \frac{1}{N-1} \sum_{j \neq i \in G} \frac{1}{L_{i,j}} \text{ and } E_{i_local} = \frac{1}{N_G(N_G-1)} \sum_{j,k \in G} \frac{1}{L_{jk}}$$

where L_{ij} is the shortest path length between node i . N is the number of nodes in graph G_i .

Small-worldness analysis

The small-worldness property of neural network is described by the clustering coefficient (C_p) and characteristic path length (L_p). The C_p is defined as the average of clustering coefficients (C_i) of all nodes in the neural network and the L_p is defined as the average of the shortest path length between any pair of nodes in the neural network. The C_{p_rand} and L_{p_rand} are defined as the mean C_p and L_p of the matched random network, respectively. The mathematical definitions are characterized as follows:

$$C(i) = \frac{2E(i)}{K_i(K_i-1)}$$

where E is the number of existing connections among nodes i and K is the degree of nodes i . The threshold of statistical significance is presented by sparsity ranges of 0.1–0.5, where the step is 0.05. The network would be considered small-world if it meets the following conditions:

$$\gamma = C_p / C_{p_rand} > 1, \lambda = L_p / L_{p_rand} \approx 1.$$

To identify differences in the FC matrix and topology properties between the two groups, two-sample t -test was

performed. For multiple comparison correction, results in FC matrices were further corrected based on the network-based analysis (NBS) where the permutation tests were repeated 1,000 times. For results in topology properties, results were further corrected based on false discovery rate (FDR) correction. The value of $p < 0.05$ was considered statistically significant.

Statistical analysis

Statistical analyses were conducted using IBM SPSS 25.0 statistics (IBM, Chicago, Illinois, United States). Values were presented as mean \pm standard error of mean (SEM). Results in ELISA measurements and RT-PCR were analyzed by one-way ANOVA followed by *Bonferroni post hoc* analysis. Results in MWM probe trials were analyzed by two-sample t -test. Results in the MWM spatial acquisition trials were analyzed by repeated measures two-way ANOVA followed by *Bonferroni post hoc* analysis. The value of $p < 0.05$ was considered statistically significant. Analysis methods for rs-fMRI data are mentioned in the appropriate subsections above.

Results

Physiological factors during rs-fMRI scanning

Physiological factors during rs-fMRI data acquisition were strictly controlled. No differences were observed in weight, heart rate (HR), respiratory rate (RR) and blood oxygen level (SpO₂) between the two groups ($p = 0.838$, $p = 0.735$, $p = 0.676$, $p = 0.283$, respectively, two-sample t -test; Table 3).

Lipopolysaccharide exposure caused short- and long-term impaired learning and spatial working memory

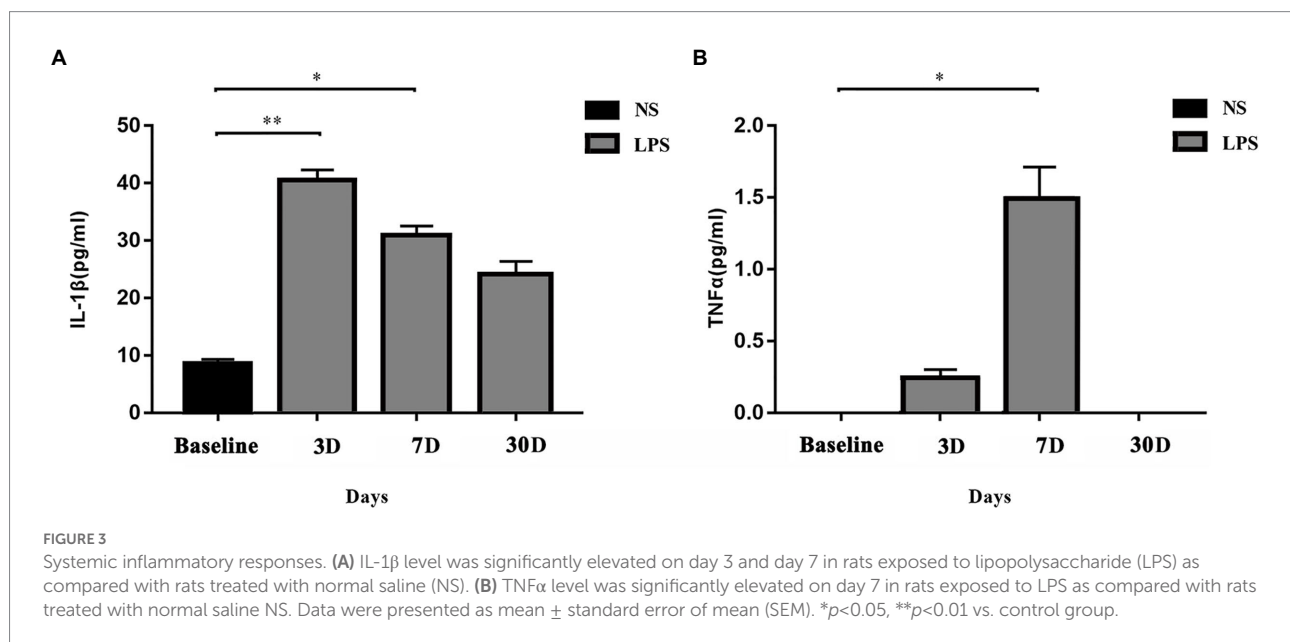
The MWM was used to determine the effects of LPS exposure on learning and spatial working memory in both short- (<7 days) and long-term (>30 days). From day 1 to day 5, significant differences were observed in rats exposed to LPS ($F_{(1,51)} = 26.309$ for treatment; $F_{(4,204)} = 73.179$ for training days, $p < 0.001$, repeated measures two-way ANOVA; Figure 2B). A significant difference was also observed for interaction between training treatment and training days ($F_{(4,204)} = 2.840$, $p = 0.025$). *Post hoc* analysis indicated that LPS caused significantly increased escape latency from day 2 to day 4 ($p < 0.001$, $p = 0.003$ and $p < 0.001$, respectively). For the probe trial on day 7, a shorter time spent in target quadrant and fewer platform crossovers ($p < 0.001$ and $p < 0.001$, respectively, two-sample t -test; Figures 2C,D) were observed in rats

³ <https://www.nitrc.org/projects/gretna>

TABLE 3 Physiological factors during rs-fMRI data acquisition.

Days	Groups	Weight (g)	HR (/min)	RR (/min)	SpO ₂ (%)
3 days	NS	752.2 ± 25.3	295.5 ± 14.8	70.9 ± 2.0	99.0 ± 0.3
	LPS	744.9 ± 24.5	302.8 ± 15.4	72.3 ± 2.4	99.4 ± 0.2
7 days	NS	748.2 ± 25.1	307.5 ± 21.3	72.5 ± 2.6	99.5 ± 0.3
	LPS	702.4 ± 18.0	308.8 ± 19.0	73.6 ± 3.3	98.9 ± 0.4
31 days	NS	772.5 ± 25.8	307.3 ± 25.1	72.1 ± 2.2	99.4 ± 0.3
	LPS	740.1 ± 23.6	306.3 ± 17.0	72.9 ± 2.6	99.2 ± 0.3

Physiological factors were carefully controlled during data acquisition. Data were analyzed by two-sample *t*-test. The value of $p < 0.05$ was considered statistically significant.



exposed to LPS. For the second acquisition trials from day 31 to day 35, significant differences were observed in rats exposed to LPS ($F_{(1,55)} = 0.021$ for treatment; $F_{(4, 220)} = 6.109$ for training days, $p = 0.021$ and $p < 0.001$, respectively, repeated measures two-way ANOVA; Figure 2E). A significant difference was also observed for interaction between training treatment and training days ($F_{(4, 204)} = 2.704$, $p = 0.031$). *Post hoc* analysis showed that rats exposed to LPS had longer escape latency on day 34 and 35 ($p = 0.009$ and $p < 0.001$, respectively). For the probe trial on day 37, a shorter time spent in the target quadrant and fewer platform crossovers were also observed for rats exposed to LPS ($p < 0.001$ and $p < 0.001$, respectively; Figures 2F,G).

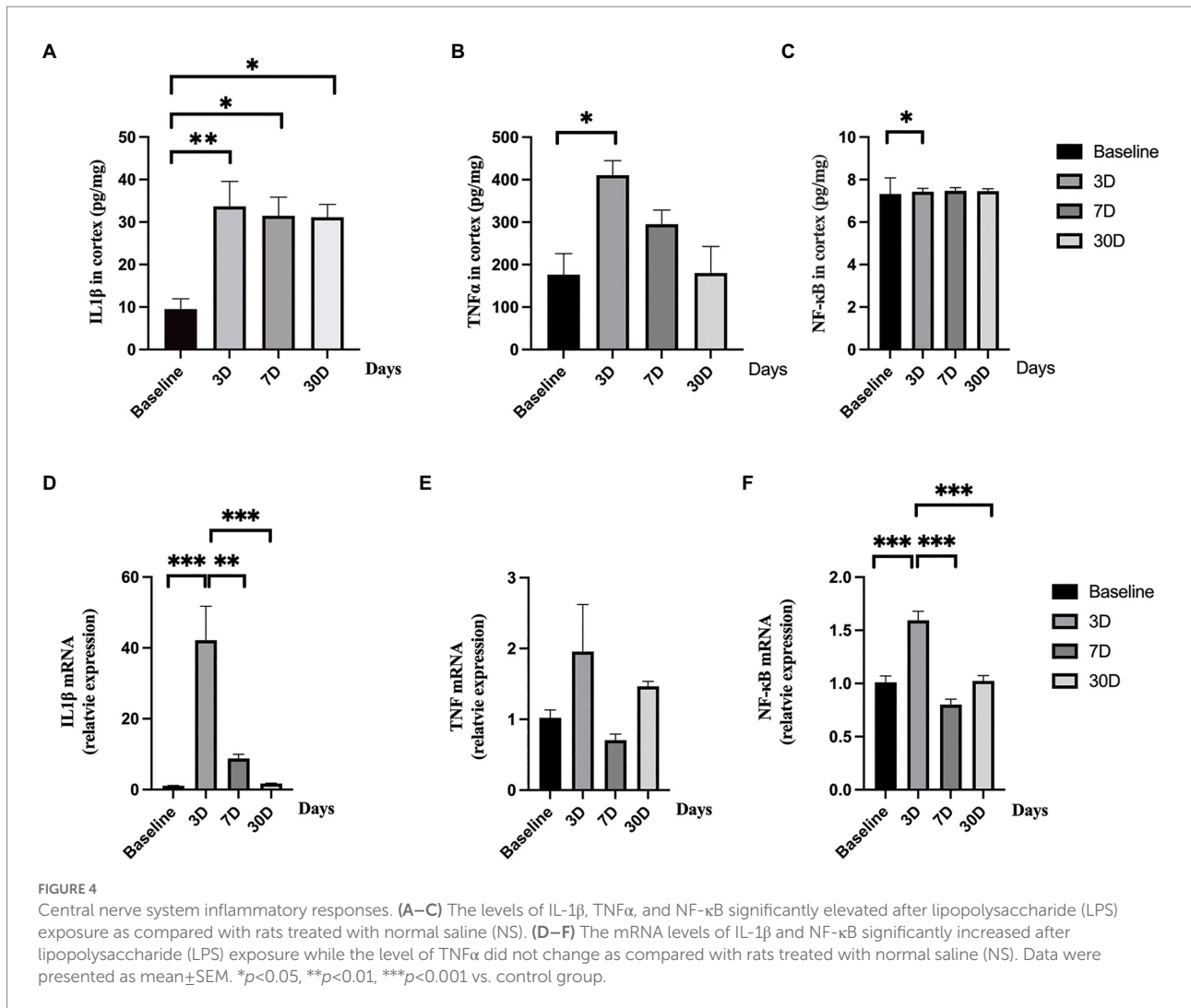
Lipopolysaccharide exposure caused increased systemic inflammatory response

Systemic levels of IL-1 β and TNF α were significantly increased in rats exposed to LPS ($p = 0.002$ and $p = 0.009$, respectively;

one-way ANOVA). IL-1 β level in rats exposed to LPS reached a peak at 3 days and remained elevated at 7 days ($p = 0.001$ and $p = 0.04$, respectively, *Bonferroni post hoc* analysis; Figure 3A). For TNF α level, a significant increase occurred at 7 days ($p = 0.02$, *Bonferroni post hoc* analysis; Figure 3B).

Lipopolysaccharide exposure caused increased inflammatory response in rat brain

To determine whether LPS exposure caused inflammatory responses in aged rat brain, proinflammatory cytokines and mRNA expressions were measured. LPS exposure caused significant increase in IL-1 β , TNF α , and NF- κ B ($p = 0.005$, 0.005 , and $p = 0.043$, respectively; one-way ANOVA; Figure 4). The secretion of IL-1 β reached a peak level 3 days, slightly decreased on day 7, and remained significantly higher on day 30 after LPS exposure ($p = 0.006$, 0.023 , and 0.026 as compared with control, *Bonferroni post hoc* analysis, Figure 4A). For TNF α and NF- κ B, they both reached peak levels on day 3 after



LPS exposure and went back to normal on day 7 and day 30 ($p = 0.013, 0.477, \text{ and } 1.000$ as compared with control for TNF α ; $p = 0.043, 0.296$ and 1.000 as compared with control for NF- κ B, *Bonferroni post hoc* analysis, [Figures 4B,C](#)). When considering mRNA expression, LPS exposure caused a significant change in IL-1 β and NF- κ B ($p < 0.001$ and $p < 0.001$, [Figures 4D,F](#)) while no significant change was observed in TNF α level ($p = 0.118$, [Figure 4E](#)). The mRNA expressions of IL-1 β and TNF α reached a peak level on day 3 after LPS exposure and fall back to almost baseline level on day 7 and day 30 ($p < 0.001$ for IL-1 β and $p < 0.001$ for NF- κ B, *Bonferroni post hoc* analysis).

Lipopolysaccharide exposure caused significant short- and long-term FC alterations In aged rat DMN

After LPS exposure, significant altered FC was temporarily observed with 13 in cortico-cortical connections and 10 in

cortical-subcortical connections in LPS group on day 3 (two-sample *t*-test with NBS corrected; [Figures 5A,B](#)). One subcortico-subcortical connections were affected (L-Hip and R-Hip). On day 7, significant altered FC was observed in rats exposed to LPS with 7 in cortico-cortical connections and 8 in cortico-subcortical connections (two-sample *t*-test with NBS corrected; [Figures 5C,D](#)). On day 31, FC remained significantly altered in rats exposed to LPS with 9 in cortico-cortical connections and 9 in cortico-subcortical connections (two-sample *t*-test with NBS corrected; [Figures 5E,F](#)).

Lipopolysaccharide exposure caused short-term instead of long-term topology alterations in aged rat neural network

All rats in both groups showed small-worldness properties for all time points ($\gamma = C_p/C_{p\text{-rand}} > 1, \lambda = L_p/L_{p\text{-rand}} \approx 1$; [Figure 6A](#)). No significant differences were observed in clustering coefficient

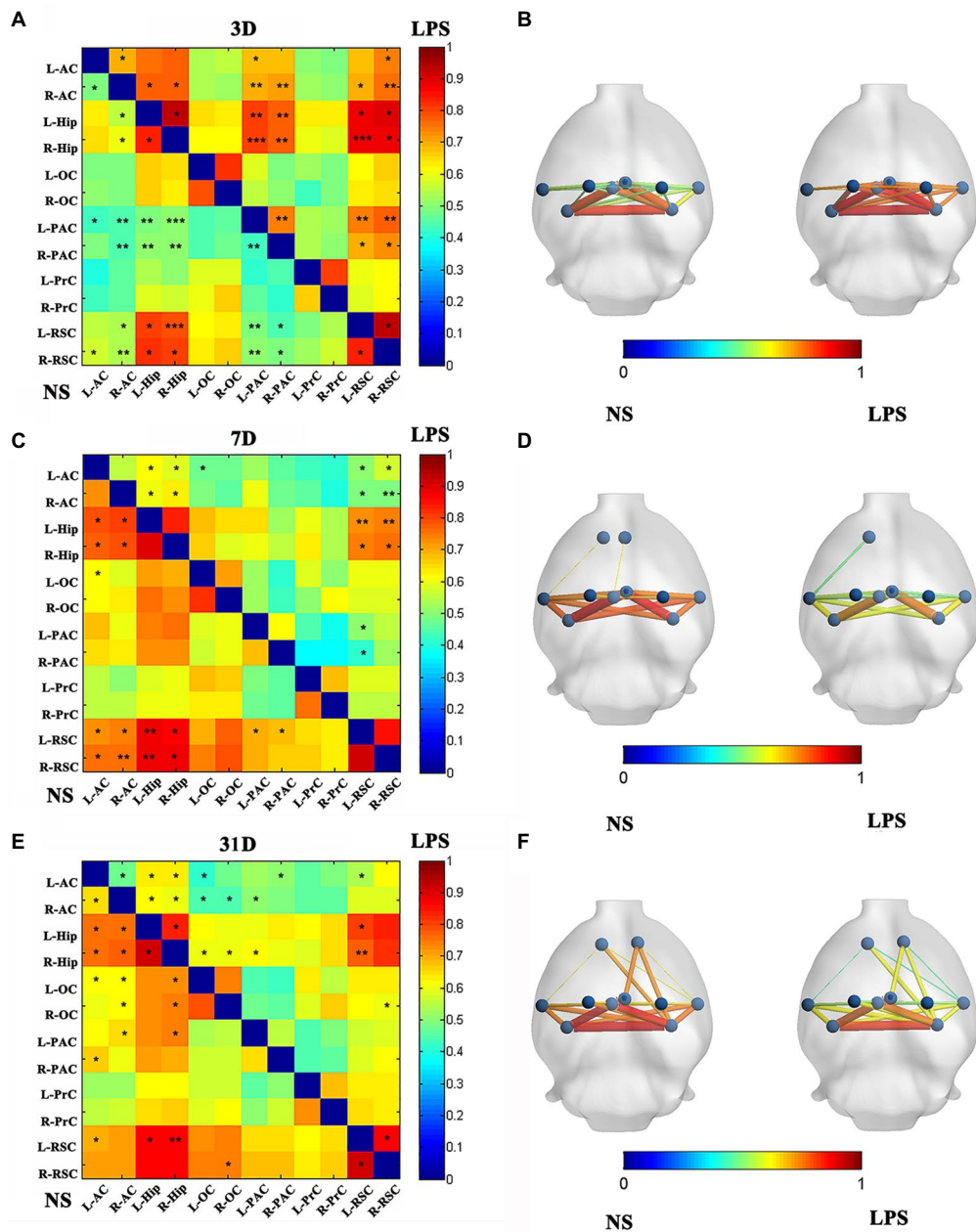


FIGURE 5 Functional connectivity (FC) in rats with lipopolysaccharide (LPS) exposure compared with control group. **(A,B)** FC value, nodes, and edges position in rats receiving LPS exposure (right) and control group (left) on day 3 after LPS exposure. **(C,D)** FC value, nodes, and edges position in rats receiving LPS exposure (right) and control group (left) on day 7 after treatment. **(E,F)** FC value, nodes, and edges position in rats receiving LPS exposure (right) and control group (left) on day 31 after treatment. Data were analyzed using two-sample *t*-test with network-based analysis correction (permutation 1,000 times). **p*<0.05, ***p*<0.01, ****p*<0.001 vs. control group.

(Figure 6B) while a significant increased shortest path length was observed in rats exposed to LPS on day 3 ($p=0.00489$, two-sample *t*-test with FDR corrected; Figure 6C).

Although lower global efficiency was observed at 3 days in rats exposed to LPS ($p=0.033$, two-sample *t*-test with FDR corrected; Figure 7A), there was no difference between LPS-exposed and control rats in local efficiency (Figure 7B). For local properties, in rats exposed to LPS, E_i was significantly lower

in the left and right occipital cortices (L-OC and R-OC) and left and right prelimbic cortices (L-PrC and R-PrC $p=0.0013$, 0.0031 , 0.019 , and 0.0013 , respectively, two-sample *t*-test with FDR corrected; Figure 5C). E_{i_local} was significantly lower in left and right occipital cortices (L-OC and R-OC; $p=0.0040$ and 0.012 , respectively, two-sample *t*-test with FDR corrected; Figure 5D). However, LPS exposure also caused higher E_i in left-parietal association cortex (L-PAC; $p=0.0054$, Figure 7C), and higher

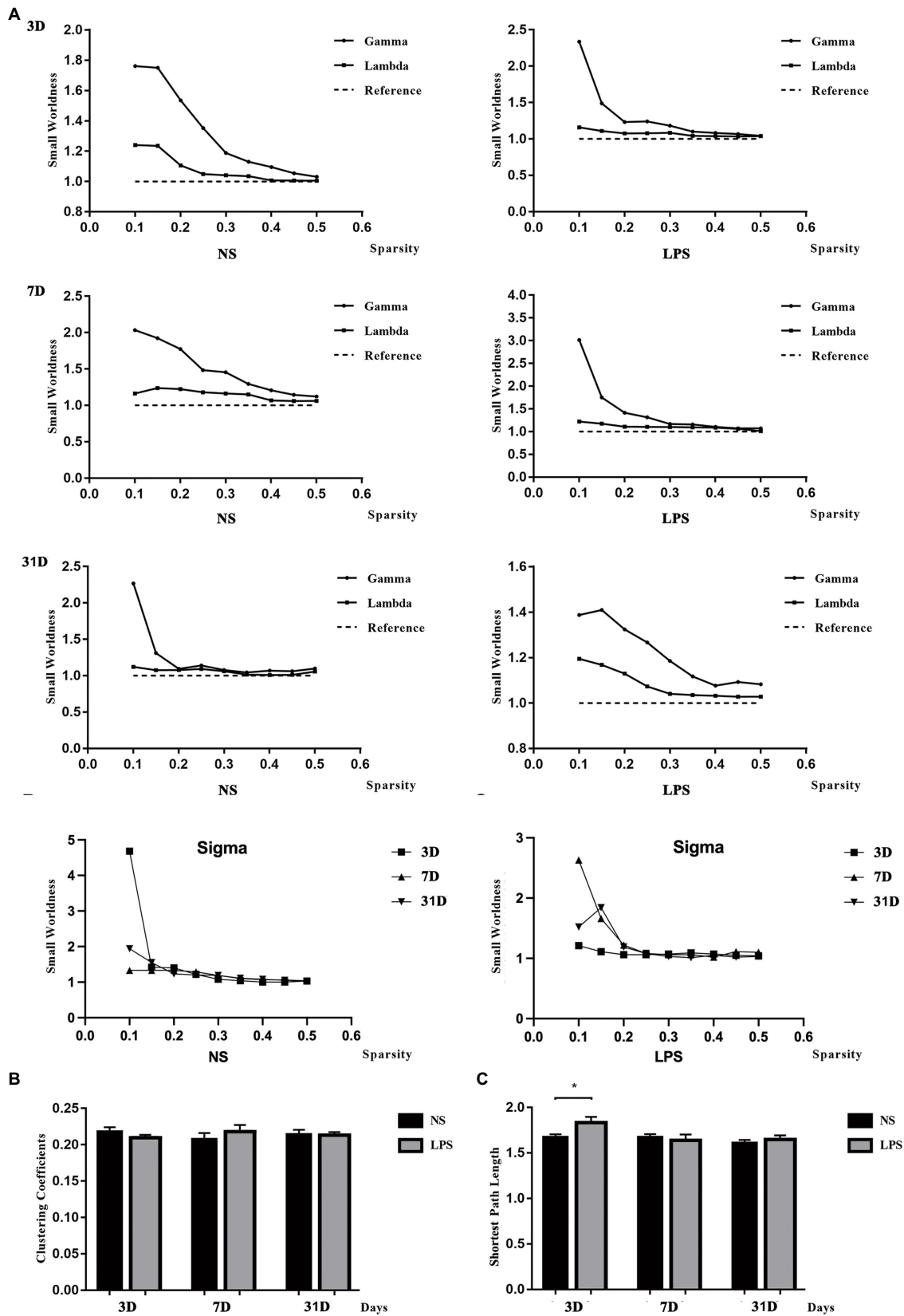
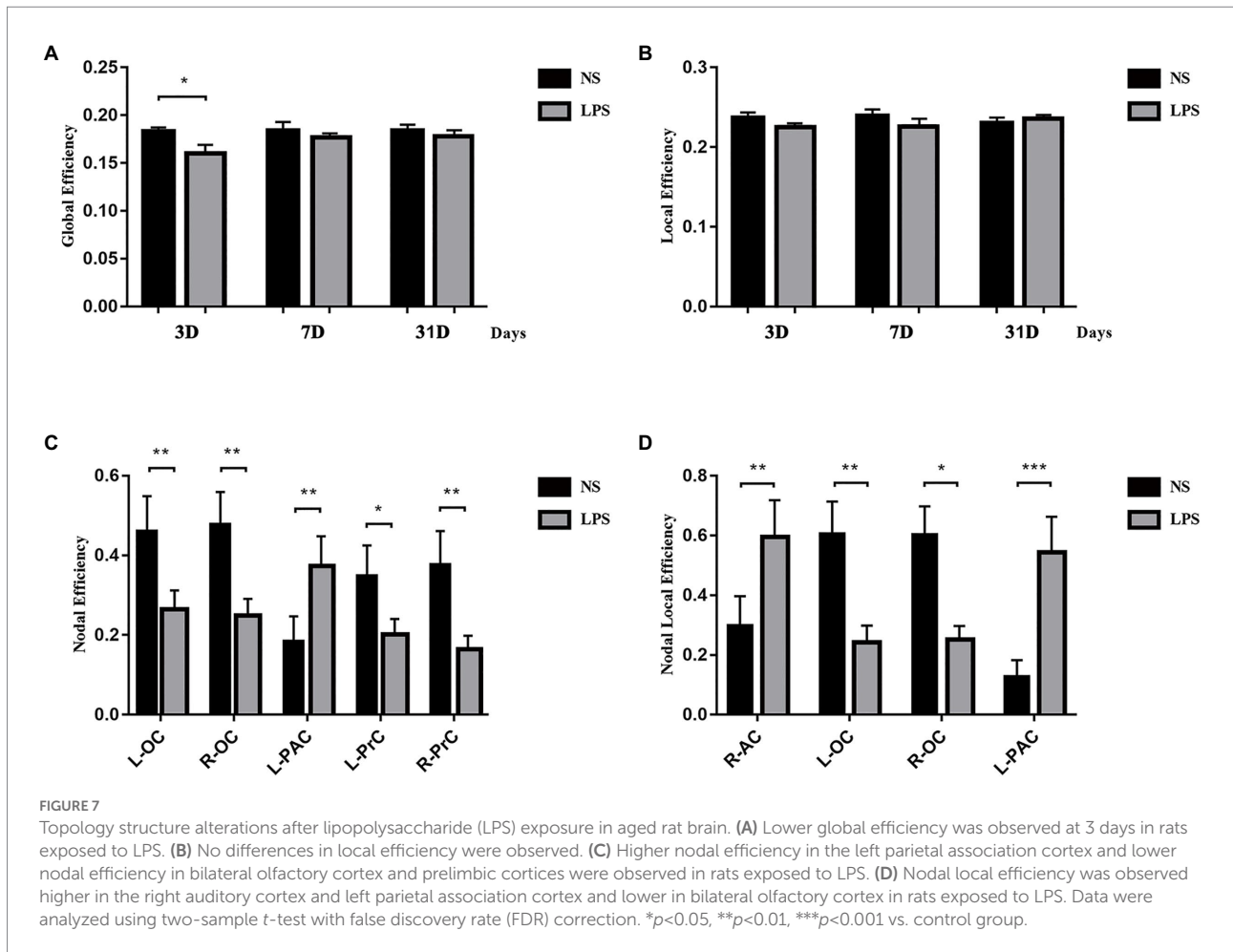


FIGURE 6
 Small-worldness in aged rat default mode network (DMN). **(A)** The DMN in lipopolysaccharide (LPS) exposed and control rats showed the small-worldness at all time points. **(B)** LPS exposure caused no alteration in clustering coefficient (C_p). **(C)** LPS exposure caused increased shortest path length (Lp) persisting for 3 days. Data were analyzed using two - sample t-test with false discovery rate (FDR) correction. $**p < 0.01$ vs. control group.



E_{i_local} in right-auditory cortex (R-AC) and L-PAC ($p=0.0067$ and 0.0001 , Figure 7D). On days 7 and 31 after LPS exposure, no significant topology changes were observed between the two groups.

Discussion

The present study demonstrated that inflammatory stress exposure in anesthesia caused altered intrinsic connectivity of the DMN, short- and long-term impairment in learning and spatial working memory, and altered short-term topology properties in aged rat brain.

Recent studies demonstrated the significance of neuroinflammation in postoperative cognitive decline (Subramaniyan and Terrando, 2019). Systemic inflammation induced by surgical trauma and neurotoxicity induced by anesthetic exposure have been proved to be major contributors (Liu et al., 2022). Our present study showed a significant increase in serum cytokines on day 3 (for IL-1 β) and day 7 (for IL-1 β and TNF α), demonstrating the occurrence of severe systemic inflammatory response. In central nerve system, significant increases of IL-1 β (up to 30 days), TNF α (within

7 days), and NF- κ B (within 7 days), indicating the existence of subsequent neuroinflammation. In order to validate the effect of neuroinflammation, the MWM was performed to test cognitive function in aged rats. The present study showed significant longer escape latency, lower time spent, and fewer crossovers in target quadrant in both MWM testing within 7 days and more than 30 days after LPS exposure, indicating that neuroinflammation induced short- and long-term cognitive dysfunction, which is consistent with our previous findings (Fu et al., 2014; Kan et al., 2016).

Altered FC in neural network is a major characteristic in cognitive dysfunction in both clinical practice (Labrenz et al., 2016; Tani et al., 2018) and preclinical experiments (Anckaerts et al., 2019; Passamonti et al., 2019). In the present study, we observed altered intrinsic connectivity in aged rat DMN on day 7 and day 31 after LPS exposure, which is consistent with clinical findings that FC in DMN is decreased in cognitive dysfunction (Qian et al., 2019; Zhao et al., 2020). Contrary to impaired MWM performance, increased intrinsic connectivity within the rat DMN was temporarily observed on day 3 after LPS exposure. Considering the severe systemic inflammation in aged rats, it could be explained by “systemic inflammation induced transient enhancement” as what was reported in

human subjects 3.5 h after inflammatory exposure (Labrenz et al., 2016), which also shown that systemic inflammation began to affect DMN intrinsic connectivity at least 3 days after exposure.

Aside from whole DMN, the Hip and RSC are two most important regions (Raichle, 2015). While both contributing to learning and memory, the Hip plays a more significant role on recent delay while the RSC is more significant in remote delay and trace conditioning (assessed by fear conditioning) in AD related studies (Todd et al., 2019). Although altered RSC-related FC (which corresponds to the post-cingulate gyrus in mankind), which was observed in A β -induced cognitive decline in human subjects (Yamashita et al., 2019), was found in our study, the Hip rather than RSC seemed to play a more significant role in the long-term (11 vs. 12 CCs, 8 vs. 10CCs, 10 vs. 5 CCs for 3 days, 7 days and 31 days, respectively). We hypothesize that the reason for this may be a greater sensitivity of the Hip to inflammation in the aged rat as compared with normal adult rats (Barrientos et al., 2015). This result demonstrates that surgery stress and anesthetic neurotoxicity-induced cognitive decline differs from dementia induced by A β accumulation, supporting the recent idea that postoperative cognitive dysfunction (POCD) and AD are associated with different transcriptome changes despite their similar clinical manifestations (Wang et al., 2022).

Meanwhile, significant Hip-related FC changes combined with impaired behavior performances existed throughout the experiment period while not all the FCs in the DMN remained changed. This finding indicated that Hip played a significant role not only in neurodegeneration but also in inflammation exposure-induced cognitive dysfunction. Our findings are consistent with previous study that the hippocampus remained severe inflammatory response in long-term cognitive dysfunction (Li et al., 2020). Impaired Hip-related FCs demonstrated neural transmission dysfunction between Hip and other DMN regions, which indicated that impaired correlation between Hip and other DMN regions might be a significant character in inflammatory-induced cognitive dysfunction. Our previous study also showed that there are significant changes in Hip-related FCs in aged rat brain although treatment had already given (Liu et al., 2021). These findings all pointed to the significance of anti-inflammatory treatment in clinical practice, which may help to prevent long-term cognitive dysfunction after anesthesia and inflammation exposure.

Besides intrinsic connectivity (FC in the DMN), topology structure in neural network is also significant in information transmission. Small-worldness, a model combining high C_p and short L_p , is a highly optional choice for studying complex networks in the setting of psychophysiological condition (Bassett and Bullmore, 2017; Miraglia et al., 2020). In the present study, rats with inflammatory exposure showed increased L_p followed with impaired behavior performances, which is similar with clinical findings that AD patients have disrupted small-worldness

properties characterized by increased L_p (Dai et al., 2019; Lella and Estrada, 2020). However, it is different that the C_p is not changed in rats with inflammatory exposure-induced cognitive dysfunction as clinical studies reported that AD patients also have decreased C_p (Wu et al., 2019; Rauchmann et al., 2021). Interestingly, a lower E_{global} was observed 3 days after LPS exposure while no change in E_{loc} was also observed in the present study. These results indicated that inflammatory stress-induced cognitive dysfunction mainly relies on causing more steps in information exchange in small-worldness neural network instead of decreasing local interconnectivity between different regions, although they all disrupt small-worldness properties. This also supports the idea that POCD induced by anesthesia and surgery is different from early stage of AD. Whether the POCD develops into AD in the future still needs further studies. For regional properties (E_i , E_{local}), LPS exposure caused both increased and decreased changes, which may be a compensation for the decrease in global information transformation. On day 7 and 31 after LPS exposure, no significant differences could be observed in topology properties, while the difference in FC remained, showing that FC alterations, rather than topology changes, may last longer in LPS-induced cognitive impairment.

Based on the results of our study, we presented a background of DMN intrinsic connectivity and topology structures after inflammatory exposure in aged rat brain, indicating short- and long-term changes in functional connectivity and topology structures. Meanwhile, our study also pointed out brain regions that played a significant role in long-term cognitive dysfunction. In the future, a treatment could be given to these rats to evaluate the effect on aged rat DMN and cognitive function in both short- and long-term, providing further evidence for clinical practice. Considering that the DMN exists across species and the components are similar, these results can be used as background data, helping to judge treatment effect and drug-target design.

There are several limitations for the present study. First, the data were collected from aged rats instead of elderly patients. The reason for doing this is that using LPS on senior mankind for inducing sepsis and long-term cognitive dysfunction may cause ethical problem. Fortunately, recent studies reported that the component of DMN in aged rat is similar with those in human beings (Smallwood et al., 2021) and the FC alteration was also observed in various conditions (Serra et al., 2020), making the aged rats an optional choice for mechanism studying. Second, no data from post-mortem subjects were acquired for background comparison. The reason for not doing this is that we have to acquire longitudinal data and the rats have to undergo MWM testing. Third, the anesthesia method may have potential influences on FC patterns in the rat DMN (Paasonen et al., 2018). However, after comparing different methods, the combination of ISO and DEX was selected because it is a proven method for DMN studies and better preserves DMN connectivity as compared with several other anesthetic methods (Lu et al., 2012; Paasonen et al., 2018).

Conclusion

The present study demonstrated inflammatory exposure in anesthesia management impairs intrinsic FC and disrupts small-worldness in aged rat DMN. Alterations in FC may be long-term while disrupted small-worldness may only be temporary. These results offer further insights into drug target design and new biomarkers for cognitive dysfunction induced by anesthesia and inflammatory stress exposure in clinical practice.

Data availability statement

The raw data supporting the conclusions of this article will be made available by the authors, without undue reservation.

Ethics statement

The animal study was reviewed and approved by Ethical Committee of Capital Medical University.

Author contributions

YL, HF (Huiru Feng) and TW: study design. YL and HF (Huiru Feng): study performance. YL, HF (Huiqun Fu) and BN: rs-fMRI data analysis. YL and HF (Huiru Feng): manuscript writing. YW, BN and TW: manuscript revision. Dr. Yang Liu and Dr. Huiru Feng contributed equally to the manuscript and shares first authorship.

Funding

This work was supported by grants from Beijing Municipal Health Commission (Jing 2019-2); Beijing municipal

References

- Anckaerts, C., Blockx, I., Summer, P., Michael, J., Hamaide, J., Kreutzer, C., et al. (2019). Early functional connectivity deficits and progressive microstructural alterations in the TgF344-AD rat model of Alzheimer's disease: a longitudinal MRI study. *Neurobiol. Dis.* 124, 93–107. doi: 10.1016/j.nbd.2018
- Avena-Koenigsberger, A., Misis, B., and Sporns, O. (2017). Communication dynamics in complex brain networks. *Nat. Rev. Neurosci.* 19, 17–33. doi: 10.1038/nrn.2017.149
- Barrientos, R. M., Kitt, M. M., Watkins, L. R., and Maier, S. F. (2015). Neuroinflammation in the normal aging hippocampus. *Neuroscience* 309, 84–99. doi: 10.1016/j.neuroscience.2015.03.007
- Bassett, D. S., and Bullmore, E. T. (2017). Small-world brain networks revisited. *Neuroscientist* 23, 499–516. doi: 10.1177/1073858416667720
- Belrose, J. C., and Noppens, R. R. (2019). Anesthesiology and cognitive impairment: a narrative review of current clinical literature. *BMC Anesthesiol.* 19:241. doi: 10.1186/s12871-019-0903-7
- Biswal, B., Yetkin, F., Haughton, V., and Hyde, J. (1995). Functional connectivity in the motor cortex of resting human brain using echo-planar MRI. *Magn. Reson. Med.* 34, 537–541. doi: 10.1002/mrm.1910340409
- Cao, Y., Yang, H., Zhou, Z., Cheng, Z., and Zhao, X. (2020). Abnormal default-mode network homogeneity in patients with mild cognitive impairment in Chinese communities. *Front. Neurol.* 11:569806. doi: 10.3389/fneur.2020.569806
- Chand, G. B., Wu, J., Hajjar, I., and Qiu, D. (2017). Interactions of the salience network and its subsystems with the default-mode and the central-executive

administration of hospitals clinical medicine development of special funding support (Code: ZYLX201706); and Beijing 215 high-level healthcare talent plan academic leader (Code: 008-0027).

Acknowledgments

The authors may express their appreciation to Shengyu Fang from Department of Neurosurgery, Beijing Tiantan Hospital, Capital Medical University for his generous help on data analysis. The authors may also express their appreciation to the staffs of Beijing Area Major Laboratory of Peptide and Small Molecular Drugs, Engineering Research Centre of Endogenous Prophylactic of Ministry of Education of China.

Conflict of interest

The authors declare that the research was conducted in the absence of any commercial or financial relationships that could be construed as a potential conflict of interest.

Publisher's note

All claims expressed in this article are solely those of the authors and do not necessarily represent those of their affiliated organizations, or those of the publisher, the editors and the reviewers. Any product that may be evaluated in this article, or claim that may be made by its manufacturer, is not guaranteed or endorsed by the publisher.

networks in normal aging and mild cognitive impairment. *Brain Connect.* 7, 401–412. doi: 10.1089/brain.2017.0509

Dai, Z., Lin, Q., Li, T., Wang, X., Yuan, H., Yu, X., et al. (2019). Disrupted structural and functional brain networks in Alzheimer's disease. *Neurobiol. Aging* 75, 71–82. doi: 10.1016/j.neurobiolaging.2018.11.005

Daiello, L. A., Racine, A. M., Yun Gou, R., Marcantonio, E. R., Xie, Z., Kunze, L. J., et al. (2019). Postoperative delirium and postoperative cognitive dysfunction: overlap and divergence. *Anesthesiology* 131, 477–491. doi: 10.1097/ALN.0000000000002729

Duprey, M. S., Devlin, J. W., van der Hoeven, J. G., Pickkers, P., Briesacher, B. A., Saczynski, J. S., et al. (2021). Association between incident delirium treatment with haloperidol and mortality in critically ill adults. *Crit. Care Med.* 49, 1303–1311. doi: 10.1097/CCM.0000000000004976

Fu, H. Q., Yang, T., Xiao, W., Fan, L., Wu, Y., Terrando, N., et al. (2014). Prolonged neuroinflammation after lipopolysaccharide exposure in aged rats. *PLoS One* 9:e106331. doi: 10.1371/journal.pone.0106331

Fuster, J. (2001). The prefrontal cortex--an update time is of the essence. *Neuron* 30, 319–333. doi: 10.1016/s0896-6273(01)00285-9

Hohenfeld, C., Werner, C. J., and Reetz, K. (2018). Resting-state connectivity in neurodegenerative disorders: is there potential for an imaging biomarker? *Neuroimage Clin.* 18, 849–870. doi: 10.1016/j.nicl.2018.03.013

Ji, M., Xia, J., Tang, X., and Yang, J. (2018). Altered functional connectivity within the default mode network in two animal models with opposing episodic memories. *PLoS One* 13:e0202661. doi: 10.1371/journal.pone.0202661

- Jing, W., Xia, Y., Li, M., Cui, Y., Chen, M., Xue, M., et al. (2021). State-independent and state-dependent patterns in the rat default mode network. *NeuroImage* 237:118148. doi: 10.1016/j.neuroimage.2021.118148
- Kan, M. H., Yang, T., Fu, H. Q., Fan, L., Wu, Y., Terrando, N., et al. (2016). Pyrrolidine. Dithiocarbamate prevents neuroinflammation and cognitive dysfunction after endotoxemia in rats. *Front. Aging Neurosci.* 8:175. doi: 10.3389/fnagi.2016.00175
- Kukla, B., Anthony, M., Chen, S., Turnbull, A., Baran, T. M., and Lin, F. V. (2022). Brain small-worldness properties and perceived fatigue in mild cognitive impairment. *J. Gerontol. A Biol. Sci. Med. Sci.* 77, 541–546. doi: 10.1093/geron/abgab084
- Labrenz, F., Wrede, K., Forsting, M., Engler, H., Schedlowski, M., Elsenbruch, S., et al. (2016). Alterations in functional connectivity of resting state networks during experimental endotoxemia – an exploratory study in healthy men. *Brain Behav. Immun.* 54, 17–26. doi: 10.1016/j.bbi.2015.11.010
- Lakshmikanth, C. L., Jacob, S. P., Chaitra, V. H., de Castro-Faria-Neto, H. C., and Marathe, G. K. (2016). Sepsis: in search of cure. *Inflamm. Res.* 65, 587–602. doi: 10.1007/s00011-016-0937-y
- Le Merre, P., Ahrlund-Richter, S., and Carlen, M. (2021). The mouse prefrontal cortex: unity in diversity. *Neuron* 109, 1925–1944. doi: 10.1016/j.neuron.2021.03.035
- Lee, Y. H., Bak, Y., Park, C. H., Chung, S. J., Yoo, H. S., Baik, K., et al. (2019). Patterns of olfactory functional networks in Parkinson's disease dementia and Alzheimer's dementia. *Neurobiol. Aging* 89, 63–70. doi: 10.1016/j.neurobiolaging.2019.12.021
- Lella, E., and Estrada, E. (2020). Communicability distance reveals hidden patterns of Alzheimer's disease. *Netw Neurosci.* 4, 1007–1029. doi: 10.1162/netn_a_00143
- Li, Z., Wei, M., Lyu, H., Huo, K., Wang, L., Zhang, M., et al. (2020). Fracture shortly before stroke in mice leads to hippocampus inflammation and long-lasting memory dysfunction. *J. Cereb. Blood Flow Metab.* 40, 446–455. doi: 10.1177/0271678X19825785
- Li, C. X., and Zhang, X. (2018). Evaluation of prolonged administration of isoflurane on cerebral blood flow and default mode network in macaque monkeys anesthetized with different maintenance doses. *Neurosci. Lett.* 662, 402–408. doi: 10.1016/j.neulet.2017.10.034
- Liang, S., Wu, S., Huang, Q., Duan, S., Liu, H., Li, Y., et al. (2017). Rat brain digital stereotaxic white matter atlas with fine tract delineation in Paxinos space and its automated applications in DTI data analysis. *Magn. Reson. Imaging* 43, 122–128. doi: 10.1016/j.mri.2017.07.011
- Lisman, J., Buzsáki, G., Eichenbaum, H., Nadel, L., Ranganath, C., and Redish, A. D. (2017). Viewpoints: how the hippocampus contributes to memory, navigation and cognition. *Nat. Neurosci.* 20, 1434–1447. doi: 10.10138/nn.4661
- Liu, X., Chen, X., Zheng, W., Xia, M., Han, Y., Song, H., et al. (2018). Altered functional connectivity of insular subregions in Alzheimer's disease. *Front. Aging Neurosci.* 10:107. doi: 10.3389/fnagi.2018.00107
- Liu, Y., Fu, H., and Wang, T. (2022). Neuroinflammation in perioperative neurocognitive disorders: from bench to the bedside. *CNS Neurosci. Ther.* 28, 484–496. doi: 10.1111/cns.13794
- Liu, Y., Fu, H., Wu, Y., Nie, B., Liu, F., Wang, T., et al. (2021). Elamipretide (SS-31) improves functional connectivity in hippocampus and other related regions following prolonged neuroinflammation induced by lipopolysaccharide in aged rats. *Front. Aging Neurosci.* 13:600484. doi: 10.3389/fnagi.2021.600484
- Lopes, R., Delmaire, C., Defebvre, L., Moonen, A. J., Duits, A. A., Hofman, P., et al. (2017). Cognitive phenotypes in Parkinson's disease differ in terms of brain-network organization and connectivity. *Hum. Brain Mapp.* 38, 1604–1621. doi: 10.1002/hbm.23474
- Lu, H., Zou, Q., Gu, H., Raichle, M. E., Stein, E. A., and Yang, Y. (2012). Rat brains also have a default mode network. *Proc. Natl. Acad. Sci. U. S. A.* 109, 3979–3984. doi: 10.1073/pnas.1200506109
- Miraglia, F., Vecchio, F., Marra, C., Quaranta, D., Alu, F., Peroni, B., et al. (2020). Small world index in default mode network predicts progression from mild cognitive impairment to dementia. *Int. J. Neural Syst.* 30:2050004. doi: 10.1143/S0129065720500045
- Nie, B., Chen, K., Zhao, S., Liu, J., Gu, X., Yao, Q., et al. (2013). A rat brain MRI template with digital stereotaxic atlas of fine anatomical delineations in paxinos space and its automated application in voxel-wise analysis. *Hum. Brain Mapp.* 34, 1306–1318. doi: 10.1002/hbm.21511
- Oliveira, M. K., Dos Santos, R. S., Cabral, L. D. M., Vilela, F. C., and Giusti-Paiva, A. (2020). Simvastatin attenuated sickness behavior and fever in a murine model of endotoxemia. *Life Sci.* 254:117701. doi: 10.1016/j.lfs.2020.117701
- Paasonen, J., Stenroos, P., Salo, R. A., Kiviniemi, V., and Grohn, O. (2018). Functional connectivity under six anesthesia protocols and the awake condition in rat brain. *NeuroImage* 172, 9–20. doi: 10.1016/j.neuroimage.2018.01.014
- Pascoal, T. A., Mathotaarachchi, S., Kang, M. S., Mohaddes, S., Shin, M., Park, A. Y., et al. (2019). Abeta-induced vulnerability propagates via the brain's default mode network. *Nat. Commun.* 10:2353. doi: 10.1038/s41467-019-10217-w
- Passamonti, L., Tsvetanov, K. A., Jones, P. S., Bevan-Jones, W. R., Arnold, R., Borchert, R. J., et al. (2019). Neuroinflammation and functional connectivity in Alzheimer's disease: interactive influences on cognitive performance. *J. Neurosci.* 39, 7218–7226. doi: 10.1523/JNEUROSCI.2574-18.2019
- Qian, W., Fischer, C. E., Churchill, N. W., Kumar, S., Rajji, T., and Schweizer, T. A. (2019). Delusions in Alzheimer disease are associated with decreased default mode network functional connectivity. *Am. J. Geriatr. Psychiatry* 27, 1060–1068. doi: 10.1016/j.jagp.2019.03.020
- Raichle, M. E. (2015). The Brain's default mode network. *Annu. Rev. Neurosci.* 38, 433–447. doi: 10.1146/annurev-neuro-071013-014030
- Rauchmann, B. S., Ersoezlue, E., Stoecklein, S., Keeser, D., Brosseron, F., Buerger, K., et al. (2021). Resting-state network alterations differ between Alzheimer's disease atrophy subtypes. *Cereb. Cortex* 31, 4901–4915. doi: 10.10193/cercor/bhab130
- Schumacher, J., Gunter, J. L., Przybelski, S. A., Jones, D. T., Graff-Radford, J., Savica, R., et al. (2021). Dementia with Lewy bodies: association of Alzheimer pathology with functional connectivity networks. *Brain* 144, 3212–3225. doi: 10.1093/brain/awab218
- Serra, L., Bruschini, M., Di Domenico, C., Mancini, M., Bechi Gabrielli, G., Bonarota, S., et al. (2020). Behavioral psychological symptoms of dementia and functional connectivity changes: a network-based study. *Neurobiol. Aging* 94, 196–206. doi: 10.1016/j.neurobiolaging.2020.06.009
- Smallwood, J., Bernhardt, B. C., Leech, R., Bzdok, D., Jefferies, E., and Margulies, D. S. (2021). The default mode network in cognition: a topographical perspective. *Nat. Rev. Neurosci.* 22, 503–513. doi: 10.1038/s41583-021-00474-4
- Sporns, O. (2018). Graph theory methods applications in brain networks. *Diagnoses Clin Neurosci.* 20, 111–121. doi: 10.31887/DCNS.2018.20/osporns
- Subramanian, S., and Terrando, N. (2019). Neuroinflammation and perioperative neurocognitive disorders. *Anesth. Analg.* 128, 781–788. doi: 10.1213/ANE.0000000000004053
- Tani, N., Yaegaki, T., Nishino, A., Fujimoto, K., Hashimoto, H., Horiuchi, K., et al. (2018). Functional connectivity analysis and prediction of cognitive change after carotid artery stenting. *J. Neurosurg.* 131, 1709–1715. doi: 10.3171/2018.7.JNS18404
- Todd, T. P., Fournier, D. I., and Bucci, D. J. (2019). Retrosplenial cortex and its role in cue-specific learning and memory. *Neurosci. Biobehav. Rev.* 107, 713–728. doi: 10.1016/j.neurobiorev.2019.04.016
- Wang, Y., Wang, L., Yuan, S., Zhang, Y., Zhang, X., and Zhou, L. (2022). Postoperative cognitive dysfunction and Alzheimer's disease: a transcriptome-based comparison of animal models. *Front. Aging Neurosci.* 14:900350. doi: 10.3389/fnagi.2022.900350
- Wang, J., Zuo, X., and He, Y. (2010). Graph-based network analysis of resting-state functional MRI. *Front. Syst. Neurosci.* 4:16. doi: 10.3389/fnsys.2010.00016
- Wu, Z., Xu, D., Potter, T., and Zhang, Y. (2019). Alzheimer's Disease Neuroimaging Initiative (2019). Effects of brain parcellation on the characterization of topological deterioration in Alzheimer's disease. *Front. Aging Neurosci.* 11:113. doi: 10.3389/fnagi.2019.00113
- Yamashita, K. I., Uehara, T., Prawiroharjo, P., Yamashita, K., Togao, O., Hiwatashi, A., et al. (2019). Functional connectivity change between posterior cingulate cortex and ventral attention network relates to the impairment of orientation for time in Alzheimer's disease patients. *Brain Imaging Behav.* 13, 154–161. doi: 10.1007/s11682-018-9860-x
- Yang, T., Velagapudi, R., and Terrando, N. (2020). Neuroinflammation after surgery: from mechanisms to therapeutic targets. *Nat. Immunol.* 21, 1319–1326. doi: 10.1038/s41590-020-00812-1
- Yang, L., Zhou, R., Tong, Y., Chen, P., Shen, Y., Miao, S., et al. (2020). Neuroprotection by dihydrotestosterone in LPS-induced neuroinflammation. *Neurobiol. Dis.* 140:104814. doi: 10.1016/j.nbd.2020.104814
- Yeshurun, Y., Nguyen, M., and Hasson, U. (2021). The default mode network: where the idiosyncratic self meets the shared social world. *Nat. Rev. Neurosci.* 22, 181–192. doi: 10.1038/s41583-020-00420-w
- Zhang, H., Chiu, P., Ip, I., Liu, T., Wong, G., Song, Y., et al. (2021). Small-world networks and their relationship with hippocampal glutamine/glutamate concentration in healthy adults with varying genetic risk for Alzheimer's disease. *J. Magn. Reson. Imaging* 54, 952–961. doi: 10.1002/jmri.27632
- Zhao, T., Quan, M., and Jia, J. (2020). Functional connectivity of default mode network subsystems in the presymptomatic stage of autosomal dominant Alzheimer's disease. *J. Alzheimers Dis.* 73, 1435–1444. doi: 10.3233/JAD-191065